Clustering effects in the exit channels of $^{13,12}C + ^{12}C$ reactions within the collective clusterization mechanism of the dynamical cluster decay model

Rupinder Kaur,[1,2] Sarbjeet Kaur,[2] BirBikram Singh,[2,*] B. S. Sandhu,[1] and S. K. Patra[3]
[1]*Department of Physics, Punjabi University, Patiala-147002, India*
[2]*Department of Physics, Sri Guru Granth Sahib World University, Fatehgarh Sahib-140406, India*
[3]*Institute of Physics, Sachivalya Marg, Bhubhaneswar-751005, India*

(Received 12 January 2020; accepted 26 February 2020; published 24 March 2020)

From the past few years, increasing experimental evidence has shown that clusters (multiple of α particles) of intermediate mass are emitted with quite large cross sections at forward angles in heavy-ion reactions. In the present work a theoretical investigation has been made to explore the role of α-clustering in $^{13,12}C + ^{12}C$ reactions populating $^{25,24}Mg^*$ compound nuclei (CN), which results in the enhanced cross sections of intermediate mass fragments (IMFs) within the collective clusterization framework of the dynamical cluster decay model (DCM). With in the formalism the experimental cross sections are reproduced using the spherical as well as deformed configurations effects included up to quadruple deformations (β_{2i}) for two nuclei having optimum orientations $\theta^{\rm opt}$. The ratio of the calculated (fission-like) yields of each isotopic fragment ^{6,7}Li, ^{7,8,9}Be obtained in the two reactions has been compared with the experimental and statistical model predictions also. The DCM calculated result is in little better comparison to the statistical models due to the inclusion of structure effects in the calculations. In the present calculations, the dynamical yields count for the preformation probability (P_0) of the IMFs within the collective clusterization process of DCM, before penetrating the scattering potential barrier. Quite interestingly, the calculated ratio of P_0 of the corresponding IMFs $P^{^{25}Mg^*}_{0(\rm IMFs)}/P^{^{24}Mg^*}_{0(\rm IMFs)}$ for the CN $^{25,24}Mg^*$ shows the trend of ratio of experimental cross sections, i.e., $\sigma^{^{25}Mg^*}_{\rm IMFs}/\sigma^{^{24}Mg^*}_{\rm IMFs}$. It is found that α-cluster structure of complimentary fragments of the IMFs under investigation plays quite a significant role in their decays.

DOI: 10.1103/PhysRevC.101.034614

I. INTRODUCTION

Clustering process appears to play a crucial role in the formation of galaxies as well as in the decay of heavy nuclei into lighter nuclei, and can be treated as extreme examples occurring in nature. Within an atomic nucleus, nucleon clusterization process which treats the nucleons as a cluster rather than free nucleons has been extensively used to explain a number of nuclear phenomena. In one of the earliest studies, the nucleus was viewed as a collection of α particles [1] and well-known examples of such nuclear clustering are the tightly bound α particle and Hoyle state of ^{12}C. The famous Ikeda diagrams have also suggested the structure of various α conjugate nuclei depending on their excitation energy. Thus, both theoretical as well as experimental [2–10] efforts are being devoted to the study of clustering phenomena in nuclei in ground state decay and as well as in the dissipative decay of excited/hot composites systems populated through the reactions involving excitation energies $\lesssim$100 MeV.

Low-energy heavy ion collisions leading to the decay products of the very-light-mass composite systems ($A = 20$–40) have been studied extensively, specifically for the composite systems in which neutron and proton numbers differ or are equal [11–13]. In this mass region the cluster structures have been studied experimentally in ^{10}Be, ^{10}B, ^{18}O, ^{22}Ne, ^{40}Ca, etc., [14,15]. Moreover, in the reactions involving α-cluster nuclei a large enhancement in yield and a resonance-like excitation function in a few outgoing channels have been noticed, for which the deep-inelastic orbiting mechanism (DIO)/quasimolecular resonance phenomena have been found to be in competition with the fusion-fission (FF) mechanism [16]. Recently, Manna *et al.* have investigated the role of α-clustering in the binary complex fragment decay of fully energy-relaxed composite systems $^{25,24}Mg^*$, populated in $^{13,12}C + ^{12}C$ reactions. The cross section of the emitted fragments ^{6,7}Li and ^{7,8,9}Be have been measured and the ratio of the obtained yields, respectively, in the case where two reactions are compared with the corresponding statistical models prediction of the same. For the set of reactions the observed enhancement in the measured yields of ^{7,8,9}Be fragments has been quoted to the α clusterization in the complementary binary fragment nuclei ^{16,17,18}O [17]. Recently, Bailey *et al.* have also shown the α-clustering in ^{18}F nucleus [18].

Theoretically, Buck *et al.* have also investigated the α-particle cluster structure in ^{18,19}F and ^{18}O [19]. Magda *et al.* have investigated that the forward emission of clusters with $2 \leqslant Z \leqslant 4$ at energies lower than 10 MeV/nucleon can be accounted for mainly due to the projectile break-up mechanism [20]. For a description of clustering in unstable nuclei, a powerful approach of antisymmetrized molecular dynamics (AMD) successfully describes clustering and deformations of

*birbikramsingh@sggswu.edu.in

light unstable nuclei [10]. The clusterization phenomenon has been very well explained within the DCM [8,9] studies as well.

Clusterization phenomenon makes an interesting case to study a few more composite nuclei in this mass region within the collective clusterization process of DCM to develop a system. With this motivation, we intend to investigate fragments emission from composite nuclei (CN) ^{25,24}Mg* formed in the reactions ^{13,12}C + ^{12}C at $E^* \approx 53.9$ MeV [17], within DCM to give a dynamical description of the mechanism in the low-energy domain. The structure information of the fragments with respect to the specific exit channels containing the complementary binary fragment as α-cluster or neighboring nuclei has been explored using their higher preformation probabilities within the clusterization approach of the model. The DCM calculated results have been compared with the available experimental data [17]. Section II briefly describes the model used. The details of the calculations and discussions are mentioned in Sec. III and the results are concluded in Sec. IV.

II. THE DYNAMICAL CLUSTER-DECAY MODEL FOR HOT AND ROTATING COMPOUND SYSTEM

The theoretical calculations have been performed using the DCM developed by Gupta and collaborators [8,9,21–28]. The model takes into account all possible decay modes of the CN via emission of light particles (LPs), $A \leqslant 4$ (results in evaporation residues), intermediate mass fragments (IMFs), $5 \leqslant A \leqslant 20$, and symmetric fission fragments (SFs) or near symmetric fission fragments (nSFs), $A/2$ (corresponds to fission). The model, based on the quantum mechanical fragmentation theory (QMFT) [25,29], defines the CN decay cross section or the fragment production cross section for different ℓ partial waves as

$$\sigma = \sum_{\ell=0}^{\ell_{\rm crit}} \sigma_\ell = \frac{\pi}{k^2} \sum_{\ell=0}^{\ell_{\rm crit}} (2\ell+1) P_0 P; \quad k = \sqrt{\frac{2\mu E_{\rm c.m.}}{\hbar^2}}, \tag{1}$$

where the preformation probability P_0 that gives significant information related to nuclear structure refers to η motion (mass asymmetry/charge asymmetry) and the penetrability P refers to R motion (the relative separation coordinate R between two nuclei or in general between two fragments), which further depends on angular momentum ℓ and temperature T. In Eq. (1), μ $(= \frac{A_1 A_2}{A_1 + A_2} m)$ is referred as reduced mass, where m is the nucleon mass.

The preformation probability $P_0(A_i) = |\psi_R(\eta(A_i))|^2 \sqrt{B_{\eta\eta}} \frac{2}{A_{\rm CN}}$ is given by the solution of the stationary Schrödinger wave equation in η, at fixed $R = R_a$,

$$\left\{ -\frac{\hbar^2}{2\sqrt{B_{\eta\eta}}} \frac{\partial}{\partial\eta} \frac{1}{\sqrt{B_{\eta\eta}}} \frac{\partial}{\partial\eta} + V(R,\eta,T) \right\} \psi^\nu(\eta) = E^\nu \psi^\nu(\eta) \tag{2}$$

with $\nu = 0, 1, 2, 3 \ldots$ referring to ground state ($\nu = 0$) and excited states ($\nu = 1, 2, 3 \ldots$) solutions and $i = 1$ or 2, for the heavy and light fragment, respectively, and assuming the Boltzmann-like occupation of excited states

$$|\psi(\eta)|^2 = \sum_{\nu=0}^{\infty} |\psi^\nu(\eta)|^2 \exp(-E^\nu/T). \tag{3}$$

Here, for deformed and oriented reaction products, R_a, which is defined as

$$R_a = R_1(\alpha_1, T) + R_2(\alpha_2, T) + \Delta R(T), \tag{4}$$

is the first turning point of the penetration path. ΔR is the temperature dependant neck length parameter. In Eq. (2) the mass parameters $B_{\eta\eta}$ are the classical hydrodynamical masses [30]. The formalism is generalized for deformed and oriented nuclei by using the radii R_1 and R_2 given by

$$R_i(\alpha_i, T) = R_{0i}(T) \left[1 + \sum_\lambda \beta_{\lambda i} Y_\lambda^{(0)}(\alpha_i) \right]. \tag{5}$$

Here, angle α_i is the angle between the symmetry axis and the radius vector of the colliding nucleus, measured in the clockwise direction with respect to the symmetry axis. The temperature dependent nuclear radii $R_{0i}(T)$ for equivalent spherical nuclei is defined as $R_{0i}(T) = [1.28A_i^{1/3} - 0.76 + 0.8A_i^{-1/3}](1 + 0.0007T^2)$ [31], and T (in MeV) related to $E^*_{\rm CN} = \frac{1}{9}AT^2 - T = E_{\rm c.m.} + Q_{\rm in}$ where $Q_{\rm in}$ is the Q value of the incoming channel.

The preformation probability P_0, presented in Fig. 2, contains the structure information of the CN which enters via the minimized fragmentation potential shown in Fig. 1 for different CN chosen, and is defined as the fragmentation potential $V_R(\eta, \ell, T)$:

$$\begin{aligned} V_R(\eta,\ell,T) = & \sum_{i=1}^{2} [V_{\rm LDM}(A_i, Z_i, T)] \\ & + \sum_{i=1}^{2} [\delta U_i] \exp\left(-T^2/T_0^2\right) \\ & + V_C(R, Z_i, \beta_{\lambda i}, \theta_i, T) + V_P(R, A_i, \beta_{\lambda i}, \theta_i, T) \\ & + V_\ell(R, A_i, \beta_{\lambda i}, \theta_i, T). \end{aligned} \tag{6}$$

Here, $V_{\rm LDM}$ is the T-dependent liquid drop model energy from Davidson *et al.* [32] and $\delta U(T)$ are the empirical shell correction from Myers and Swiatecki [33], also made T-dependent to vanish exponentially with $T_0 = 1.5$ MeV [34]. V_C, V_P, and V_ℓ are, respectively, the T-dependent Coulomb potential, the nuclear proximity potential [35], and angular momentum part of the interaction as given in [25]. The deformation parameters of the nuclei $\beta_{\lambda i}$ are taken from the tables of Moller *et al.* [36], for β_{2i}, the orientations θ_i are the 'optimum' orientations of the 'hot' fusion processes which can also refer to a compact configuration, which means the interaction radius is smallest but barrier is highest.

The penetrability P or the tunneling probability in Eq. (1) is calculated as the WKB tunneling probability,

$$P = \exp\left[\frac{-2}{\hbar} \int_{R_a}^{R_b} \sqrt{2\mu[V(R) - V(R_a)]} dR \right], \tag{7}$$

solved analytically [37] with R_a and R_b as the first and second

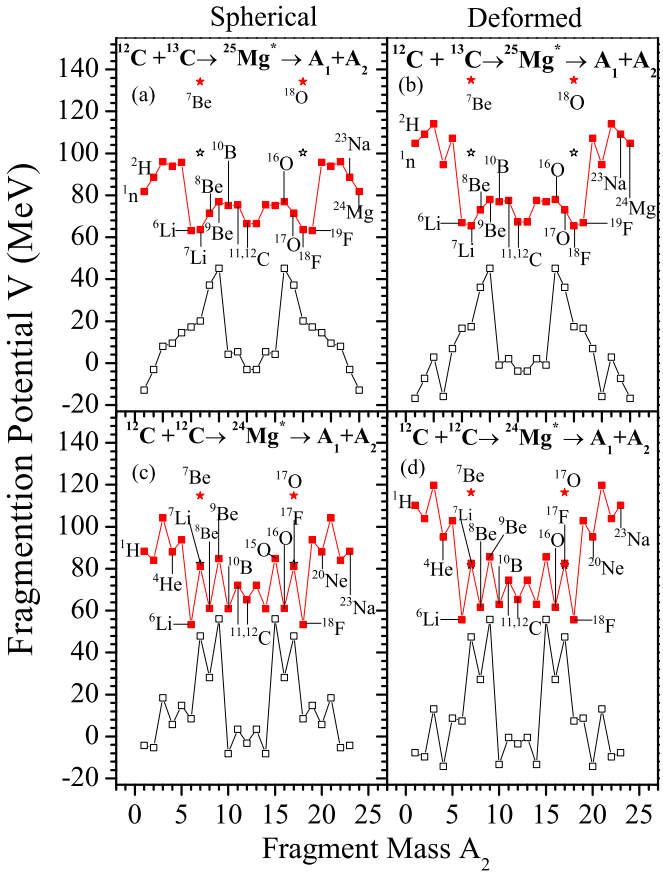

FIG. 1. The variation of fragmentation potential with fragment mass using spherical and quadruple deformations (β_{2i}) for the decay of compound nuclei ^{24,25}Mg* at $E^* \approx 53.9$ MeV, at extreme ℓ values ($\ell = 0$ and $\ell_c = 21$ for ^{24}Mg* and $\ell = 0$ and $\ell_c = 22$ for ^{25}Mg*).

turning point, satisfying

$$V(R_a) = V(R_b) = Q_{\rm eff} = {\rm TKE}(T). \tag{8}$$

The potential $V(R_a)$ can be looked upon as the effective, positive Q value, $Q_{\rm eff}(T, \ell)[= {\rm TKE}(T)]$, for the decay of a hot compound nucleus, like $Q_{\rm out}$ in the case of spontaneous ($T = 0$) cluster decay [21]. As we do not know how to add ℓ effects in the binding energies, the ℓ dependency of R_a is defined by $V(R_a) = Q_{\rm eff}(T, \ell = 0)$, which means that R_a is the same for all ℓ values and that $Q_{\rm eff}(T, \ell) = V(R_a, \ell)$. As the value of angular momentum ℓ increases, the $Q_{\rm eff}$ increases, hence $V(R_a, \ell)$ increases. So, R_a defined by Eq. (4) acts like a parameter through ΔR, the neck length parameter, which assimilates the deformation, and neck formation effects. The dynamics of the neck region generally are quite different when the two nuclei approach and rebound from each other. Here, in the present work, the variation of the neck-length parameter for the rebound state is sensitive to the compound nucleus mass and its excitation energy, inclusion of shape parameters, etc., ΔR vary smoothly from above barrier to below-barrier energies, always remaining within the range of proximity potential (2 fm). Now, using Eq. (8), $R_b(\ell)$ is given by the ℓ dependent scattering potential at fixed T,

$$V(R, T, \ell) = [Z_H Z_L e^2/R(T)] + V_P(T) + V_\ell(T), \tag{9}$$

which is normalized to the exit channel binding energy. The choice of R_a [equivalently, ΔR in Eq. (4)] allows us to define, equivalently, the barrier lowering parameter, ΔV_B, which simply relates $V(R_a, \ell)$ and the top of the barrier $V_B(\ell)$, for each ℓ, as shown in Fig. 3:

$$\Delta V_B = V(R_a, \ell) - V_B(\ell). \tag{10}$$

Here, $V(R_a, \ell)$ represents the actual barrier used for the penetration and $V_B(\ell)$ corresponds to the top barrier position. Note that ΔV_B appears as a negative quantity, $V(R_a, \ell)$ being always smaller than $V_B(\ell)$, implying that the barrier actually used to reproduce the cross sections is effectively lowered. The barrier lowering ΔV_B, associated with hindrance phenomenon, is contained in fitted ΔR values.

III. CALCULATIONS AND DISCUSSIONS

The analysis of low energy heavy ion induced reactions dynamics has been performed within the dynamical cluster decay model for the reactions ^{13,12}C + ^{12}C. The calculations are performed for spherical and quadruple deformed nuclei having hot compact configurations. The experimental cross sections of reactions populating ^{25,24}Mg* have been reproduced, using neck length parameter (ΔR) as only free parameter, at $E^*_{\rm CN} \approx 53.9$ MeV. The cross sections are obtained from the model using fragmentation potential, preformation probability, scattering potential, and penetration probability, calculated from different codes of the DCM. This section describes the role of the above-mentioned variables to obtain the cross sections and the involved dynamics.

The first important step of the model is the fragmentation potential calculation. The interaction potential as mentioned earlier also is comprised of T-dependent liquid drop model energy, empirical shell correction and Coulomb potential, the nuclear proximity potential, and angular momentum part. The fragmentation process as a function of fragment mass A of the decaying ^{25}Mg* nuclei is shown in Figs. 1(a) and 1(b) using spherical and quadruple deformation (β_{2i}) configurations at extreme angular momentum values and similarly for ^{24}Mg* as shown in Figs. 1(c) and 1(d). It can be noticed that, in case of ^{25}Mg* at $\ell = 0\hbar$ the LPs are more minimized in comparison to IMFs but with the increasing ℓ values the trend changes and now the IMFs are more pronounced in comparison to LPs. But the LPs from neutron rich compound nucleus ^{25}Mg* are competing even at higher ℓ values with the other fragments. Also, with the inclusion of deformation effects the potential energy surfaces of the LPs or their complimentary fragments are more affected at (i.e., less minimized) higher ℓ value, while the other IMFs are less affected. Similar observations are noticed for the case of ^{24}Mg* but at higher angular momenta the LPs do not compete with IMFs which is in contrast to the observations of ^{25}Mg*. It can be noticed here that the decay for both the systems is asymmetric.

Now, among the interested exit channels or IMFs, i.e., ^{6,7}Li and ^{7,8,9}Be, the fragments ^{6,7}Li in the exit channel of the ^{13}C + ^{12}C $\rightarrow$ ^{25}Mg* $\rightarrow$ ^{6,7}Li + ^{19,18}F reaction leads to ^{19,18}F as complimentary fragments, while the ^{12}C + ^{12}C $\rightarrow$ ^{24}Mg* $\rightarrow$ ^{6,7}Li + ^{18,17}F reaction leads to ^{18,17}F as complimentary fragments. It can be observed that ^{6}Li is more minimized

in the case of ^{24}Mg* in comparison to ^{25}Mg*, while for the ^{7}Li case it is more minimized in ^{25}Mg* than ^{7}Li of ^{24}Mg*. It can be noticed that in the case of ^{25}Mg* the complimentary fragments ^{19,18}F are competing with each other and are highly minimized especially for higher angular momenta values. Whereas the fragment ^{17}F in the case of ^{24}Mg* is not minimized at all in comparison to ^{19,18}F. This may be due to the absence of α-cluster structure in the case of ^{17}F.

In the exit channel for the IMF ^{7}Be for reactions $^{13,12}\mathrm{C} + {}^{12}\mathrm{C} \rightarrow {}^{25,24}\mathrm{Mg}^* \rightarrow {}^{7}\mathrm{Be} + {}^{18,17}\mathrm{O}$, ^{18,17}O are the complimentary fragments and ^{7}Be is more favored for ^{24}Mg* having lower fragmentation potential than for ^{25}Mg*. Also, the ^{7}Be fragments in both compound nuclei are not as minimized as for the case of ^{7}Li. Hence, the fragments will be preformed accordingly in the further decay process.

Among the isotopes of Be, ^{8}Be in the case of $^{13}\mathrm{C} + {}^{12}\mathrm{C} \rightarrow {}^{25}\mathrm{Mg}^* \rightarrow {}^{8}\mathrm{Be} + {}^{17}\mathrm{O}$ is less favored in comparison to ^{8}Be in the case of $^{12}\mathrm{C} + {}^{12}\mathrm{C} \rightarrow {}^{24}\mathrm{Mg}^* \rightarrow {}^{8}\mathrm{Be} + {}^{16}\mathrm{O}$ as in the former case the exit channel is ^{17}O while it is ^{16}O for the latter compound nucleus. Among these the exit channels of ^{24}Mg* i.e., ^{8}Be and ^{16}O both are well-known α-cluster nuclei. Hence, they are more pronounced. Similarly, for the exit channel of $^{13}\mathrm{C} + {}^{12}\mathrm{C} \rightarrow {}^{25}\mathrm{Mg}^* \rightarrow {}^{9}\mathrm{Be} + {}^{16}\mathrm{O}$ with one of outgoing fragment ^{9}Be having a corresponding complementary fragment as ^{16}O has a relatively lesser fragmentation potential in contrast to $^{12}\mathrm{C} + {}^{12}\mathrm{C} \rightarrow {}^{24}\mathrm{Mg}^* \rightarrow {}^{9}\mathrm{Be} + {}^{15}\mathrm{O}$ which has ^{15}O as a complementary fragment, which may be again due to the presence of an α-cluster nucleus in ^{16}O. These results are further reflected through the preformation probability graph as shown in Figs. 2(a)–2(d). It can be observed that the fragments with a 4α-cluster nucleus in the exit channel have decent preformation probabilities.

The next step is the calculation of the scattering potentials of the preformed fragments. The scattering potentials for both compound nuclei, decaying through the ^{9}Be exit channel at extreme ℓ values, is shown in Figs. 3(a)–3(d). The in-built property of barrier modification is depicted for the extreme values of angular momenta for both the used configurations. R_a and R_b correspond to the first and second turning points, for the respective exit channels. It is seen that the lowering of the barrier (ΔV_B) decreases with an increase in ℓ values, thus the penetration of the fragment is affected accordingly. Figures 4(a) and 4(b) shows ΔV_B as a function of fragment mass. The barrier lowering for different exit channels decides the penetration probability (P) of the respective fragments and is quite evident from ΣP of fragments in Figs. 5(c) and 5(d) where it can be observed that the inverse trend of ΔV_B is followed by ΣP. As in the case of ^{7}Be the ΔV_B is less so its ΣP is more, etc.

As discussed in Figs. 1(a)–1(d) and 2(a)–2(d) that the minimized fragments have higher preformation probability, Figs. 5(a) and 5(b) presents the calculated ℓ-summed up preformation probability, ΣP_0 as a function of A_2 also shows the same trend. The effect of deformations is quite small on the magnitude of the values of ΣP_0 but the pattern behavior for the different fragments remains the same as for the spherical case as shown in Fig. 5(a). It is to be noted that in fission of light systems the scission point closely resembles the saddle point [38]. It is evident from figure Figs. 5(a) and 5(b) that

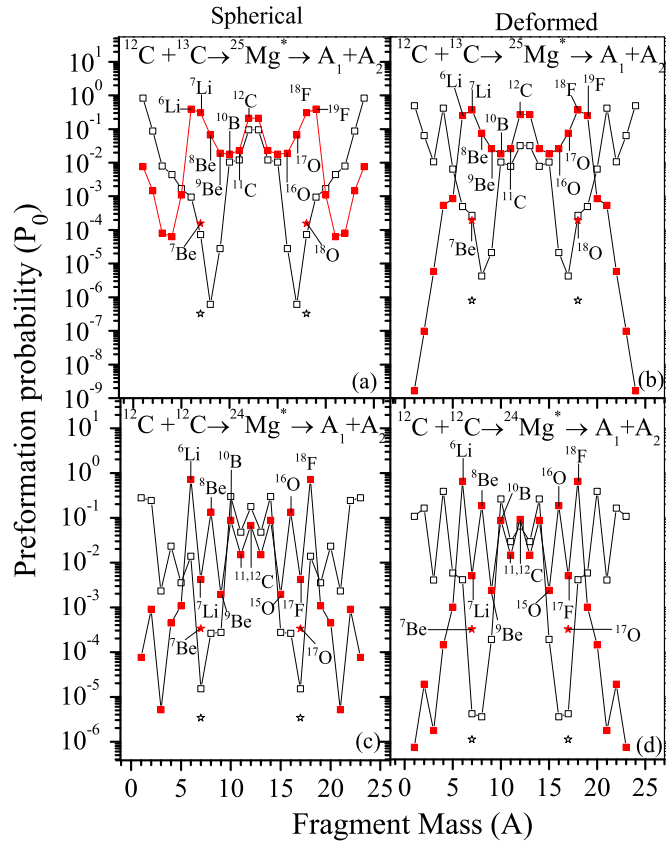

FIG. 2. The variation of preformation with fragment mass using spherical and quadruple deformations (β_{2i}) for the decay of compound nuclei ^{24,25}Mg* at $E^* \approx 53.9$ MeV, at extreme ℓ values ($\ell = 0$ and $\ell_c = 21$ for ^{24}Mg* and $\ell = 0$ and $\ell_c = 22$ for ^{25}Mg*).

the ΣP_0 of ^{7}Li and ^{9}Be is greater in the case of ^{25}Mg* in comparison to ^{24}Mg*, where as, the ΣP_0 of fragments ^{6}Li, ^{7}Be, and ^{8}Be is greater in the case of ^{24}Mg* in comparison to ^{25}Mg*. These respective higher values of the ΣP_0 result in the larger cross sections values of respective fragments, as the cross sections follow the behavior of ΣP_0, that is, the highly preformed fragment contributes a maximum towards the cross section as shown in Figs. 5(e) and 5(f). Thus, the trend in experimental data is due to ΣP_0. Figures 5(c) and 5(d) represents the ΣP of various fragments for both the chosen configurations. Here, it can be noticed again that the deformations have little effect on the ΣP of the fragments. Moreover, the values of ΣP are more or less similar for both the compound systems under study except for ^{7}Li, thereby indicating that the necessary nuclear structure information is contained in P_0 not in P and, hence, the cross sections also follow the behavior of P_0.

Finally, Fig. 6 shows the ratio of total cross sections of the decay of CN ^{25}Mg* and ^{24}Mg* formed in the $^{13,12}\mathrm{C} + {}^{12}\mathrm{C}$ reactions, respectively. The advantage of considering the ratio rather than the absolute cross section for comparison is that the effects of major experimental and computational biases are totally eliminated in the process and it brings out the physics issues more unequivocally to the forefront [17]. In this plot, the solid triangle represents the experimental data, open and

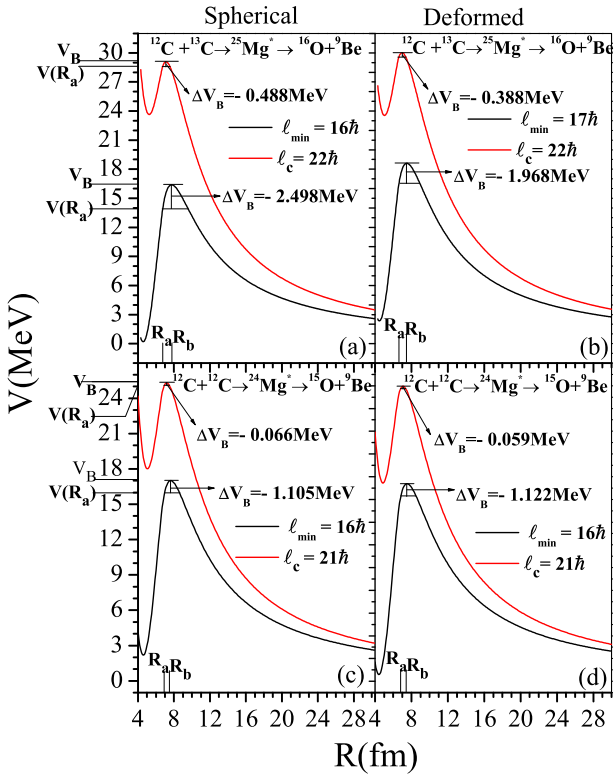

FIG. 3. The variation of scattering potential with R(fm), at $\ell_{\min}$ and ℓ_c using spherical and quadruple deformations (β_{2i}) for one of the exit channels of compound nuclei ^{24,25}Mg* at $E^* \approx 53.9$ MeV.

solid circles represent the DCM calculations whereas the open square and open triangle depicts the statistical model calculations. The calculated ratios are in fair agreement with the experimental one and is clearly evident from Table I, where

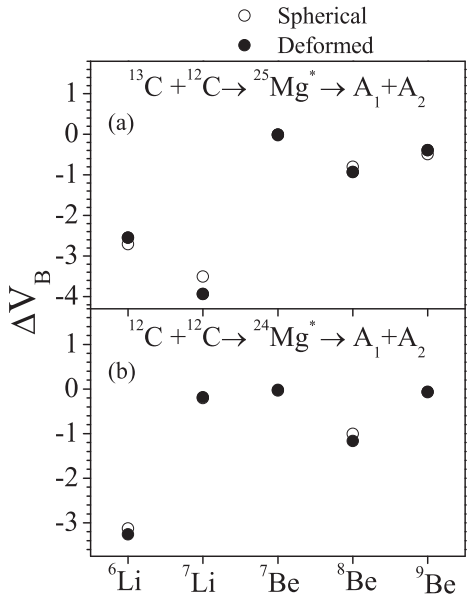

FIG. 4. The variation of ΔV_B, as a function of fragment mass (A_2) at ℓ_c using spherical and quadruple deformations (β_{2i}) for all the exit channel of compound nuclei ^{24,25}Mg* at $E^* \approx 53.9$ MeV.

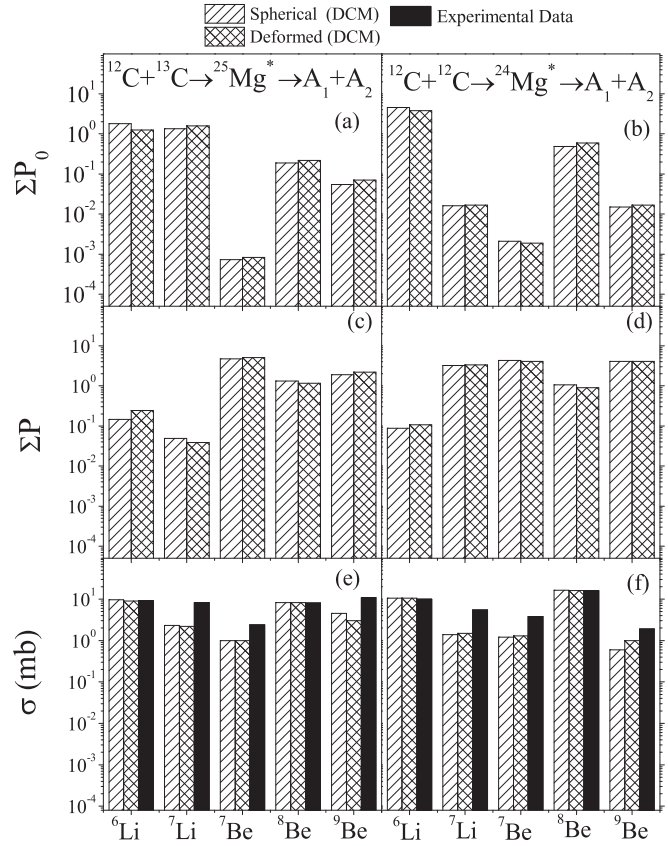

FIG. 5. The ℓ-summed preformation probability ΣP_0 [shown in (a), (b)], penetration probability ΣP [shown in (c), (d)] and cross sections σ [shown in (e), (f)] as a function of fragment mass number (A_2) calculated for different values of ℓ for the compound nuclei ^{24,25}Mg* at $E^* \approx 53.9$ MeV.

the ΔR used in both the spherical and deformed configurations in fitting the yield and their ratio of decaying CN ^{25}Mg* and ^{24}Mg* are mentioned.

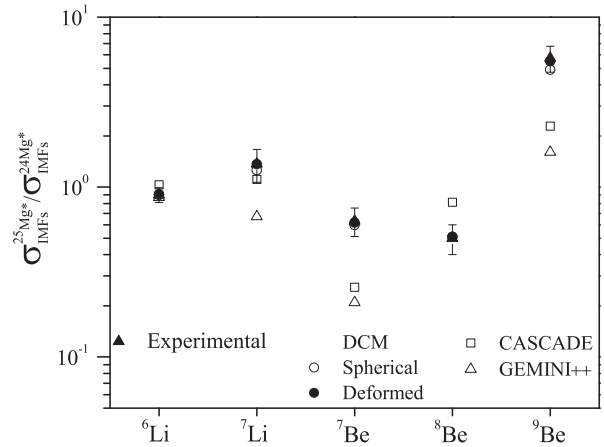

FIG. 6. The ratio of cross sections σ of the compound nucleus ^{25}Mg* with respect to compound nucleus ^{24}Mg*, also the DCM calculated cross sections are compared with experimental and statistical models.

TABLE I. The experimental and DCM-calculated IMFs cross section ($\sigma_{\rm IMFs}$) ratios of a ^{25}Mg* and ^{24}Mg* compound system considering the spherical and deformed fragmentation path.

	$^{13}C+^{12}C \rightarrow {}^{25}Mg^* \rightarrow A_1+A_2$		$^{12}C+^{12}C \rightarrow {}^{24}Mg^* \rightarrow A_1+A_2$		$\sigma^{25Mg^*}_{IMFs}/\sigma^{24Mg^*}_{IMFs}$ $\sigma^{25Mg^*}_{IMFs}/\sigma^{24Mg^*}_{IMFs}$		
	ΔR(fm)		ΔR(fm)		DCM		
IMFs	Sph.	Def.	Sph.	Def.	Sph.	Def.	Exp.
^{6}Li	0.74	0.97	0.65	0.81	0.900	0.905	0.901
^{7}Li	0.68	0.705	1.68	1.72	1.5	1.56	1.513
^{7}Be	1.78	1.86	1.76	1.78	6.0	6.3	6.316
^{8}Be	1.47	1.48	1.45	1.46	0.51	0.51	0.5
^{9}Be	1.6	1.68	1.85	1.9	4.9	5.5	5.737

For the ^{6}Li fragment emission in reactions $^{12}C+^{12}C \rightarrow {}^{24}Mg^* \rightarrow {}^6Li+{}^{18}F$ and $^{13}C+^{12}C \rightarrow {}^{25}Mg^* \rightarrow {}^6Li+{}^{19}F$ the ΣP_0 of ^{6}Li in the case of ^{24}Mg* is higher in comparison to the ΣP_0 of ^{6}Li in the case of ^{25}Mg*, so its yield is expected to be higher, also its counterpart, i.e., ΣP is low so their ratio as shown in Fig. 7 (for all the fragments results) leads to the ratio of σ near to 1. The complimentary fragment ^{19}F is a cluster of $2n+p+4\alpha$, whereas ^{18}F is $n+p+4\alpha$ the possibility of the presence of two unpaired nucleons in case ^{18}F may have also influenced the yield. In the case of ^{7}Li emission the trend of ΣP_0 and ΣP is just opposite and hence the cross section yields are affected accordingly.

The ΣP_0 of the fragment ^{7}Be in the case of the exit channel of $^{12}C+^{12}C \rightarrow {}^{24}Mg^* \rightarrow {}^7Be+{}^{17}O$ is more than ^{25}Mg* hence, its cross section value is more. The complimentary fragment in the case of ^{24}Mg* is ^{17}O which is a cluster of $n+4\alpha$, whereas for ^{25}Mg* it is ^{18}O which has $2n+4\alpha$ clusterization, hence the presence of only an unpaired neutron in ^{17}O may have resulted in a higher yield. Further for ^{8}Be fragments emission, $^{12}C+^{12}C \rightarrow {}^{24}Mg^* \rightarrow {}^9Be+{}^{16}O$, the ^{8}Be and its complimentary fragment are ^{8}Be(2α) and ^{16}O(4α), which is a well-known cluster nucleus, which may result in an enhancement in the measured yield, while for ^{25}Mg* the complementary fragment is ^{17}O, which is a clear signature of the dominant role played by the cluster structure. Moreover, the higher ΣP_0 of the fragments in the case of ^{24}Mg* leads to more yield. Similarly, it can be conjectured for the emission of the ^{9}Be fragment also for which complimentary fragments are reversed. Here, the DCM calculated result is in little better comparison due to inclusion of structure effects in the calculations.

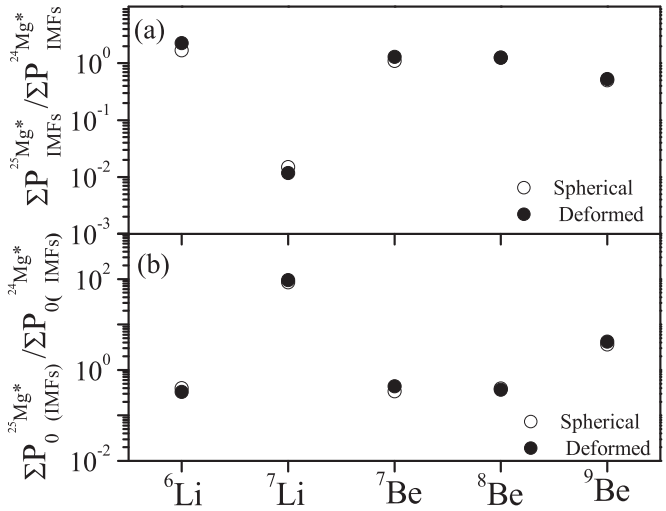

FIG. 7. The ratio of ΣP and ΣP_0 of IMFs of the compound nucleus ^{25}Mg* with respect to compound nucleus ^{24}Mg*.

IV. SUMMARY

The collective clusterization framework of the dynamical cluster decay model has been applied to study the role of α-clustering in $^{13,12}C+^{12}C$ reactions populating ^{25,24}Mg* compound nuclei. The experimental cross sections are reproduced using the spherical as well as deformed configurations effects included up to quadruple deformations (β_{2i}) for two nuclei having optimum orientations $\theta^{\rm opt}$. The calculated ratios are in fair agreement with the experimental data due to inclusion of structure effects in the calculations. The IMFs contribution from both the CN ^{25,24}Mg* remains dominant especially at the higher angular momenta values. But for neutron rich ^{25}Mg* the LPs shows a competing behavior. The inclusion of deformations affects the LPs and their complimentary fragments and a little effect is observed on the IMFs region.

It is found that the α-cluster structure of the complimentary fragments plays an important role in its enhanced preformation probability with respect to other fragments. These enhanced P_0 are evident in ΣP_0 of the fragments also and the values accordingly effect the yields of the respective fragments. The calculated ratio of P_0 of the IMFs $P^{^{25}Mg^*}_{0(IMFs)}/P^{^{24}Mg^*}_{0(IMFs)}$ for the CN ^{24,25}Mg* shows the trend of the ratio of experimental cross sections, i.e., $\sigma^{^{25}Mg^*}_{IMFs}/\sigma^{^{24}Mg^*}_{IMFs}$, thereby indicating that the necessary nuclear structure information is contained in P_0. Using the relativistic mean field theory, we intend to further explore the effects of microscopic masses and radii on the reactions dynamics of the cases studied here.

ACKNOWLEDGMENT

One of us (R.K.) acknowledges the Theoretical Nuclear Physics Research Group, Department of Physics, Sri Guru Granth Sahib World University, Fatehgarh Sahib for the support.

[1] L. Rutherford, J. Chadwick, C. D. Ellis *et al.*, Proc. R. Soc. London A **136**, 735 (1932).

[2] H. Morinaga, Phys. Rev. **101**, 254 (1956); M. Chernykh, H. Feldmeier, T. Neff, P. von Neumann-Cosel, and A. Richter, Phys. Rev. Lett. **98**, 032501 (2007).

[3] O. S. Kirsebom, M. Alcorta, M. J. G. Borge *et al.*, Phys. Rev. Lett. **108**, 202501 (2012); T. K. Rana, S. Bhattacharya, C. Bhattacharya *et al.*, Phys. Rev. C **88**, 021601(R) (2013).

[4] M. Girod and P. Schuck, Phys. Rev. Lett. **111**, 132503 (2013).

[5] L. Morelli, G. Baiocco, M. D'Agostino *et al.*, J. Phys. G **41**, 075107 (2014); **41**, 075108 (2014).

[6] A. Camaiani, G. Casini, L. Morelli *et al.*, Phys. Rev. C **97**, 044607 (2018).

[7] B. Borderie, Ad. R. Raduta, G. Ademard *et al.*, Phys. Lett. B **755**, 475 (2016).

[8] BirBikram Singh, in *Proceedings of the DAE-BRNS Symposium on Nuclear Physics*, Vol. 61 (2016), p. 510, http://www.sympnp.org/proceedings/.

[9] M. Kaur, B. B. Singh, S. K. Patra, and R. K. Gupta, Phys. Rev. C **95**, 014611 (2017).

[10] H. Horiuchi, Lect. Notes Phys. **818**, 57 (2010); Y. Kanada-En'yo and M. Kimura, *ibid.* **818**, 129 (2010).

[11] A. Szantode Toledo, M. M. Coimbra, N. Added, R. M. Anjos, N. Carlin Filho, L. Fante, Jr., M. C. S. Figueira, V. Guimares, and E. M. Szanto, Phys. Rev. Lett. **62**, 1255 (1989).

[12] M. M. Coimbra, R. M. Anjos, N. Added *et al.*, Nucl. Phys. A **535**, 161 (1991).

[13] S. Kundu, C. Bhattacharya, K. Banerjee *et al.*, Phys. Rev. C **85**, 064607 (2012).

[14] G. V. Rogachev, M. L. Avila, A. N. Kuchera *et al.*, Prog. Theor. Phys. Suppl. **196**, 184 (2012); J. Phys.: Conf. Ser. **569**, 012004 (2014).

[15] T. Yahmaya *et al.*, Phys. Lett. B **306**, 1 (1993); M. Freer and A. C. Merchant, J. Phys. G **23**, 261 (1997); G. V. Rogachev, V. Z. Goldberg, T. Lönnroth *et al.*, Phys. Rev. C **64**, 051302(R) (2001); E. D. Johnson, G. V. Rogachev, V. Z. Goldberg *et al.*, Eur. Phys. J. A **42**, 135 (2009).

[16] D. Shapira, J. L. C. Ford, J. Gomez del Campo, R. G. Stokstad, and R. M. De Vries, Phys. Rev. Lett. **43**, 1781 (1979); D. Shapira *et al.*, Phys. Rev. C **26**, 2470 (1982); Phys. Lett. B **114**, 111 (1982).

[17] S. Manna, T. K. Rana, C. Bhattacharya *et al.*, Phys. Rev. C **94**, 051601(R) (2016).

[18] S. Bailey, M. Freer, T. Kokalova, S. Cruz, H. Floyd, and D. J. Parker, Phys. Rev. C **90**, 024302 (2014); S. Bailey, M. Freer, Tz. Kokalova *et al.*, J. Phys.: Conf. Ser. **569**, 012053 (2014).

[19] B. Buck and A. A. Pilt, Nucl. Phys. A **80**, 133 (1977); B. Buck and H. Friedrich, *ibid.* **290**, 205 (1977).

[20] M. T. Magda, A. Pop, and A. Săndulescu *et al.*, J. Phys. G: Nucl. Phys. **11**, L75 (1985).

[21] R. K. Gupta, M. Balasubramaniam, R. Kumar, D. Singh, C. Beck, and W. Greiner, Phys. Rev. C **71**, 014601 (2005).

[22] B. B. Singh, M. K. Sharama, R. K. Gupta, and W. Greiner, Int. J. Mod. Phys. E **15**, 699 (2006).

[23] B. B. Singh, M. K. Sharma, and R. K. Gupta, Phys. Rev. C **77**, 054613 (2008).

[24] S. Kanwar, M. K. Sharma, B. B. Singh, R. K. Gupta *et al.*, Int. J. Mod. Phys. E **18**, 1453 (2009).

[25] R. K. Gupta, S. K. Arun, R. Kumar, and M. Bansal, Nucl. Phys. A **834**, 176c (2010); R. K. Gupta, Lect. Notes Phys. **818**, 223 (2010).

[26] M. Kaur, B. B. Singh, M. K. Sharma, and R. K. Gupta, Phys. Rev. C **92**, 024623 (2015).

[27] R. Kaur, M. Kaur, V. Singh, S. Kaur, B. B. Singh, and B. S. Sandhu, Phys. Rev. C **98**, 064612 (2018).

[28] M. Kaur, B. B. Singh, M. K. Sharma, and R. K. Gupta, Nucl. Phys. A **969**, 14 (2018).

[29] R. K. Gupta *et al.*, Phys. Rev. Lett. **35**, 353 (1975); A. Săndulescu, R. K. Gupta *et al.*, Phys. Lett. B **60**, 225 (1976); R. K. Gupta *et al.*, *ibid.* **67**, 257 (1977).

[30] H. Kröger and W. Scheid, J. Phys. G **6**, L85 (1980).

[31] G. Royer and M. Mignen, J. Phys. G: Nucl. Part. Phys. **18**, 1781 (1992).

[32] N. J. Davidson, S. S. Hsiao, J. Markram, H. G. Miller, and Y. Tzeng, Nucl. Phys. A **570**, 61c (1994).

[33] W. Myers and W. J. Swiatecki, Nucl. Phys. **81**, 1 (1966).

[34] A. S. Jensen and J. Damgaard, Nucl. Phys. A **203**, 578 (1973).

[35] J. Blocki, J. Randrup, W. J. Swiatecki, and C. F. Tsang, Ann. Phys. (NY) **105**, 427 (1977).

[36] P. Moller, J. R. Nix, W. D. Myers, and W. J. Swiatecki, At. Data Nucl. Data Tables **59**, 185 (1995).

[37] S. S. Malik and R. K. Gupta, Phys. Rev. C **39**, 1992 (1989).

[38] T. Matsuse, C. Beck, R. Nouicer, and D. Mahboub, Phys. Rev. C **55**, 1380 (1997); S. J. Sanders, A. Szanto de Toledo, and C. Beck, Phys. Rep. **311**, 487 (1999).